A Test Structure for Analyzing Self-Heating Induced Distortion in On-Chip Current Sensing Resistors

Ma, H.; Karmakar, S.; Zhang, H.; Liu, Y.; Guo, H.; Berkhout, M.; Fan, Q.

DOI
10.1109/ICMTS63811.2025.11068913

Publication date
2025

Document Version
Final published version

Published in
Proceedings of the 2025 IEEE 37th International Conference on Microelectronic Test Structures (ICMTS)

A Test Structure for Analyzing Self-Heating Induced Distortion in On-Chip Current Sensing Resistors

Heng Ma[1], Shoubhik Karmakar[1], Huajun Zhang[1], Yuyan Liu[1], Haidong Guo[2], Marco Berkhout[3], Qinwen Fan[1]
[1]Delft University of Technology, Delft, The Netherlands
[2]ams OSRAM, Plano, USA
[3]Monolithic Power Systems, Enschede, The Netherlands
Email: H.Ma-5@tudelft.nl

2025 IEEE 37th International Conference on Microelectronic Test Structures (ICMTS) | 979-8-3315-3169-0/25/$31.00 ©2025 IEEE | DOI: 10.1109/ICMTS63811.2025.11068913

***Abstract*—This paper presents a test structure for a 27 mΩ diffusion current sensing resistor, designed to analyze distortion caused by self-heating in audio power amplifiers. A parallel Kelvin connection minimizes parasitic effects, reducing resistance error to 0.4% and temperature coefficient error to 0.7%. A diode-based temperature sensor array enables accurate measurement of temperature variations, allowing the characterization of HD3 with an inaccuracy of <1.4 dB. Eventually, the HD3 is compensated by at least 15 dB through the sensed average temperature.**

Keywords—diffusion, current sensing, distortion, self-heating, Kelvin connection

I. Introduction

Integrated shunt-based current sensing is crucial in audio power amplifiers for smart speaker control [1-5]. The sense resistor is expected to have low distortion (THD+N < -68dB) to compensate for the non-ideality of the loudspeakers [1]. Considering the temperature effect, the voltage drop across the sense resistor (V_{SENSE}) is expressed as $V_{SENSE} = I \cdot R_0 (1 + tc \cdot (T_0 + T_{AC}))$ [6], where I is the current through the resistor, R_0 is the sheet resistance, tc is the temperature coefficient of the resistor, and T_{AC} is the temperature variation due to self-heating, which is a function of I^2. Then, a component of $R_0 \cdot tc \cdot I^3$ is generated on V_{SENSE}, resulting in third-harmonic distortion (HD3) [7-8], as depicted in Fig. 1(a). The HD3 can be expressed as:

$$HD3 = 20\lg(tc \cdot T_{AC\_RMS}) \quad (1)$$

where T_{AC_RMS} is the RMS value of T_{AC}. Unfortunately, this distortion cannot be simulated directly in SPICE because the T_{AC_RMS} is unknown. Without T_{AC_RMS}, it's challenging to design the on-chip resistor to the target linearity across different current frequencies and amplitudes. Additionally, to handle up to 30 W output power delivered from the power amplifier, the sense resistor needs to pass a current as high as 4 A [9-10]. It requires a large resistor width for safe current density, which leads to current spreading. Fig. 1(b) illustrates the layout of an on-chip resistor. Due to current spreading, different locations of the N (P) terminal exhibit unequal potentials, such as V_{N1} and V_{N2} [11]. This complicates the selection of accurate points to measure the voltage drop across the sense resistor. Furthermore, the large resistor area causes temperature gradients across the resistor, with different locations exhibiting different temperatures, such as T_1 at location 1 and T_2 at location 2 in Fig. 1(c), making it challenging to accurately detect the temperature of the entire resistor [12].

II. Arhitecture

To address the aforementioned issues, this paper proposes a test structure for the sense resistor, as shown in the circuit diagram in Fig. 2, incorporating a parallel Kelvin connection and a diode array. The parallel Kelvin connection minimizes parasitic effects from connection metals and vias, ensuring a more accurate measurement of the voltage drop across the resistor. Additionally, the diode-based temperature sensor array is uniformly integrated into the sense resistor to determine the average temperature and characterize the distortion from self-heating.

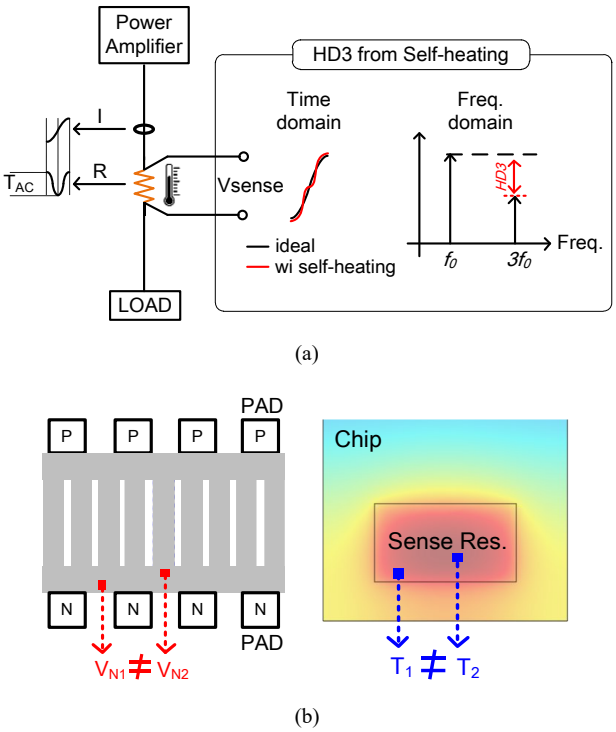

Fig.1. The HD3 of V_{SENSE} from self-heating of the sense resistor (a), the potential difference in different locations (b), and the temperature gradient across the sense resistor (c).

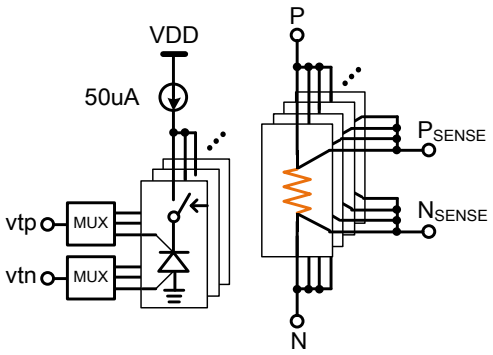

Fig. 2. Circuit diagram of the proposed test structure.

III. CIRCUIRT IMPLEMENTATION

A. Sense Resistor Type Selection

The resistance of the sense resistor is designed to be 27 mΩ, chosen as a compromise between power consumption and dynamic range. Table I compares the simulated non-idealities of different resistor types with the same resistance and chip area, including their temperature coefficient and voltage coefficient (vc), which contribute to the temperature effect [13] and saturation effect [13–15], respectively. The N-type unsilicide diffusion resistor demonstrates the best overall performance. It exhibits the lowest temperature coefficient among all resistor types. Although the P-type unsilicide poly resistor is widely used due to its low tc, this only holds with a long enough length in this process, which leads to a large chip area. When implemented as a sense resistor with the same chip area as the diffusion one, its temperature effect also becomes comparable. Furthermore, compared to other types of unsilicide resistors, the N-type unsilicide diffusion resistor exhibits at least 2× lower vc. This is critical because the saturation effect introduces additional HD3 [14], as described by: $g = g_0 (1 + vc \cdot (V_{SENSE})^2)$, where g is the transconductance of the sense resistor [15].

TABLE I. COMPARISON OF DIFFERENT TYPES OF RESISTORS

Resistor type	Silicide?	Temperature coefficient	Voltage coefficient
N-type diffusion	No	1 × (1250ppm/°C)	1 × (1400ppm/V)
	Yes	3 ×	1 ×
P-type diffusion	No	1 ×	2 ×
	Yes	3 ×	1 ×
N-type poly	No	1 ×	2 ×
	Yes	3 ×	6 ×
P-type poly	No	1 ×	4 ×
	Yes	3 ×	6 ×
Metal	/	3 ×	0
N-well	/	1.5 ×	4 ×

B. Sense Resistor Implementation

The sheet resistance of the unsilicide diffusion resistor is 83 Ω in this process, leading to an L/W of 0.0036 for a 27 mΩ resistance. The final resistor implementation consists of 7686 unit resistors, each with a L_{UNIT}/W_{UNIT} of 5 µm/2 µm. The L_{UNIT} is chosen as 5 µm to mitigate the saturation effect [10, 12] induced HD3 lower than -87 dB in the worst case (current amplitude = 4 A) , as shown in Fig. 3. It makes the saturation effect negligible compared with the linearity requirement [1]. The layout of the sense resistor is shown in Fig. 4. Each unit resistor has four terminals: the plus terminal (P), the minus terminal (N), and their Kelvin sense terminals (P_{SENSE} and N_{SENSE}). The Kelvin contacts are inserted after the current flows in at the P terminals, and before the current flows out at the N terminals. This removes the parasitic resistance of the vias from the sensed voltage. All unit resistors are arranged in a rectangle measuring 300 µm × 600 µm, with their respective terminals connected using multi-layer metals.

In this configuration, the sense resistor can be modeled as a grid in Fig. 5. The parasitic resistance from the metal connection between different Kelvin terminals ($R_{P1\sim k}$, $R_{N1\sim k}$) contributes to the main errors. The resistance error from the first connection between unit resistors R_{U0} and R_{U1} can be expressed as:

$$e_1 = \frac{R_{U0}//(R_{U1} + R_{P1} + R_{N1})}{R_{U0}//R_{U1}} - 1 \quad (2)$$

where R_{U0}, R_{U1} are designed 207.5 Ω, and R_{P1}, R_{N1} are designed 0.1ohm. Then $e1$ can be calculated as 0.048%. The error increases gradually when extending this to multiple parallel connections, becoming 0.4% eventually. Fig. 6 illustrates the simulated resistance in pre-simulation, post-simulation without parallel Kelvin connection, and post-simulation with parallel Kelvin connection. The results show that this method can decrease resistance error from 28% to 0.4%, and tc error from 18% to 0.7%.

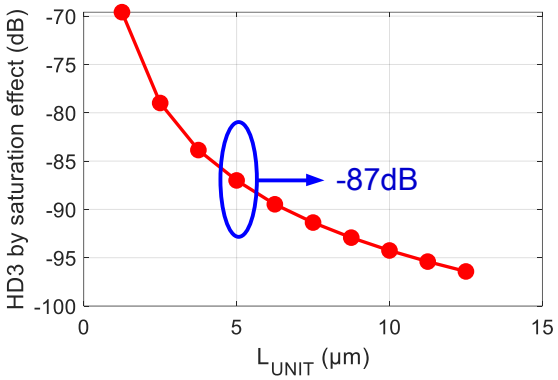

Fig. 3. Simulated HD3 caused by saturation effect with different unit resistor length when current amplitude is 4A.

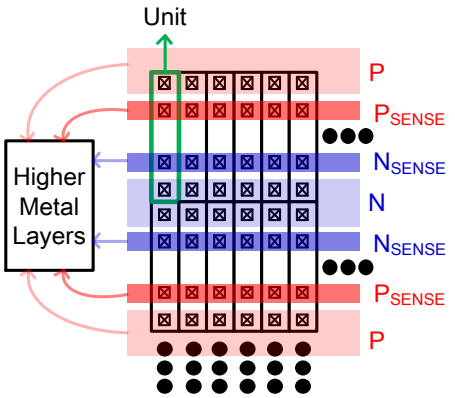

Fig. 4. The layout of the sense resistor with parallel Kelvin connection.

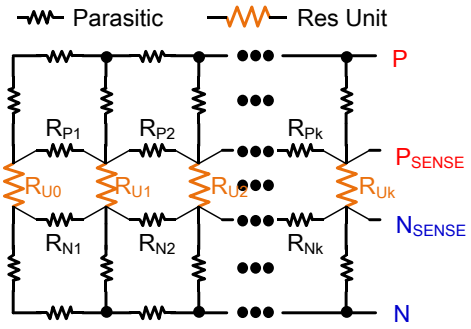

Fig. 5. Equivalent circuit of the sense resistor with parasitic resistance from metals and vias.

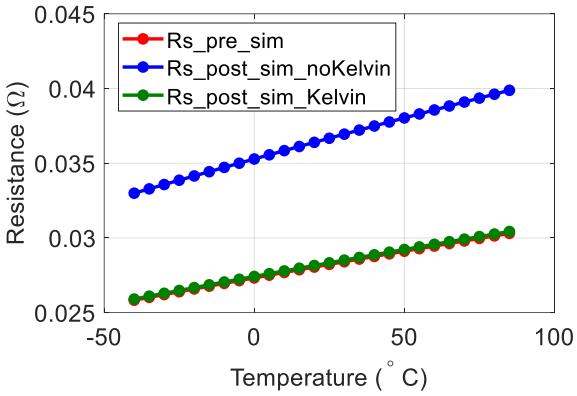

Fig. 6. The sense resistor's resistance versus temperature in pre-simulation, post-simulation without Kelvin connection, and post-simulation with parallel Kelvin connection.

C. Diode-based Temperature Sensor Array

According to (1), knowing T_{AC_RMS} is crucial to calculate HD3. However, since the sense resistor covers a large layout area, self-heating creates a temperature gradient across the resistor [9]. To improve the temperature sensing accuracy, a diode-based temperature sensor array consisting of 25 units is inserted into the resistor, as illustrated in Fig. 7. These diode units are spaced 60 µm apart, and the sensed temperatures are averaged offline to enhance measurement accuracy.

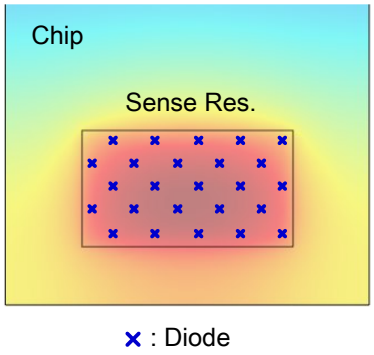

Fig. 7. The diode array to monitor the average temperature of the sense resistor.

IV. Measurement

The test structure was fabricated in a 180-nm process, and a microphotograph of the die is shown in Fig. 8. The sense resistor is located on the bottom side of the die, with the diode array distributed within it. While the bias and logic circuits are placed on the top side.

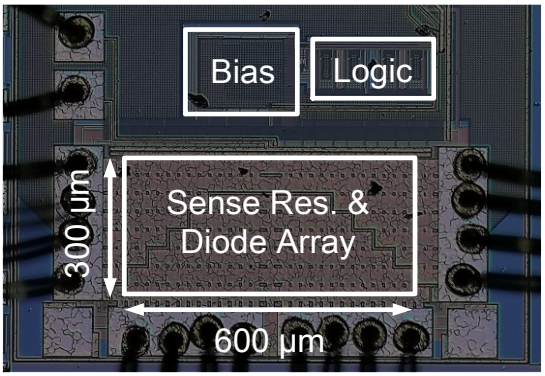

Fig. 8. Die micrograph.

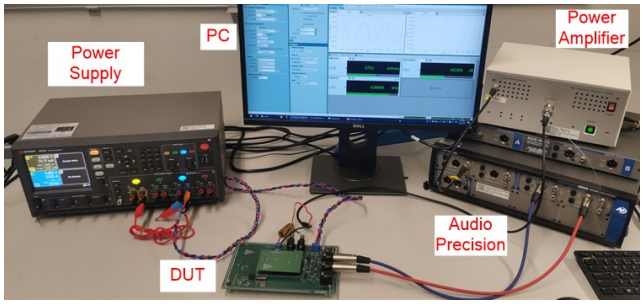

Fig. 9. Measurement setup.

The measurement setup is shown in Fig. 9. The power amplifier delivers current to the sense resistor in the DUT with varying frequencies and amplitudes. The power supply provides power voltage for the bias and logic circuits. The transient temperature and HD3 are then measured using Audio Precision. The measurement data is read and collected by the PC.

Fig. 10 presents the measured transient current and temperature sensed by the diode array when the current frequency is 200 Hz and the amplitude is 2 A. The transient temperature varies at twice the frequency of the transient current, which is related to the power consumption. From these measurements, T_{AC_RMS} is observed, and the theoretical HD3 can be calculated using (1). Fig. 11 shows the temperature sensed by 25 different diodes with a 2 A/200 Hz input current. Putting the diode in different locations can make a T_{AC_RMS} sensing error, leading to a maximum 7 dB HD3 calculation difference. The error can be mitigated to 0.15 dB by averaging those results. Fig. 12 depicts the relationship between the averaged T_{AC_RMS} measured by the diode array and signal frequency in different current amplitudes. The T_{AC_RMS} decreases with frequency due to the thermal filtering effect [13]. The high-frequency temperature is attenuated by the small thermal constant of the silicon substrate. The T_{AC_RMS} increases in larger amplitude because of more power consumption and more self-heating. Fig. 13 illustrates the measured and calculated HD3 versus current frequency across various current amplitudes. The HD3 of the sense resistor can be calculated with an inaccuracy of 1.4 dB over a current amplitude range of up to 4 A and a frequency range of 20 Hz to 6 kHz, which explains the distortion mechanism of the measured HD3. By compensating the measured HD3 with the measured average temperature through the diode array, an improvement of at least 15 dB over current frequencies and amplitudes is achieved, as shown in Fig. 14.

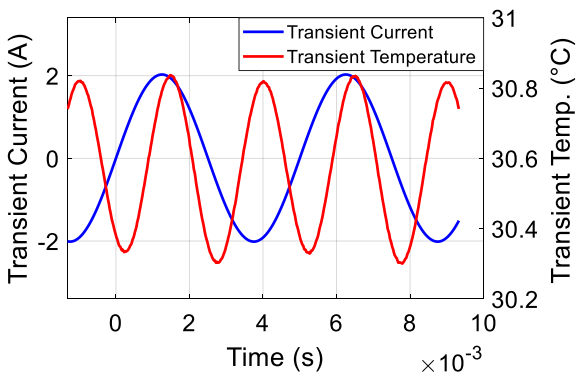

Fig. 10. Measured transient current and transient temperature with a current frequency of 200 Hz and a current amplitude of 2 A.

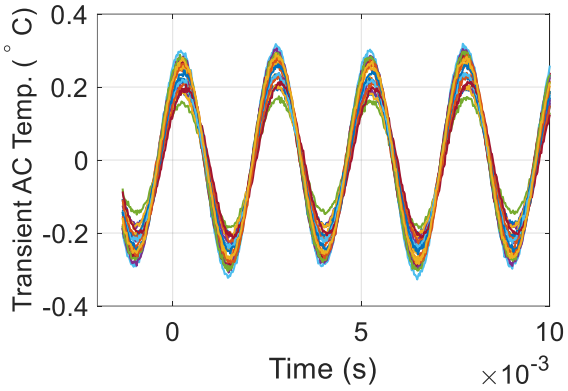

Fig. 11. Measured transient temperature of 25 different diodes with a current frequency of 200 Hz and a current amplitude of 2 A.

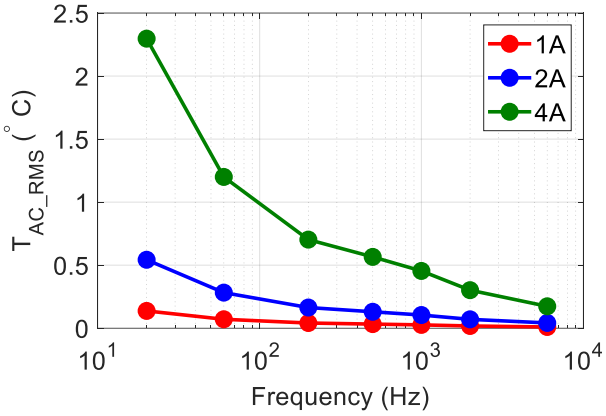

Fig. 12. Averaged T_{AC_RMS} measured by the diode array versus current frequency in different current amplitudes.

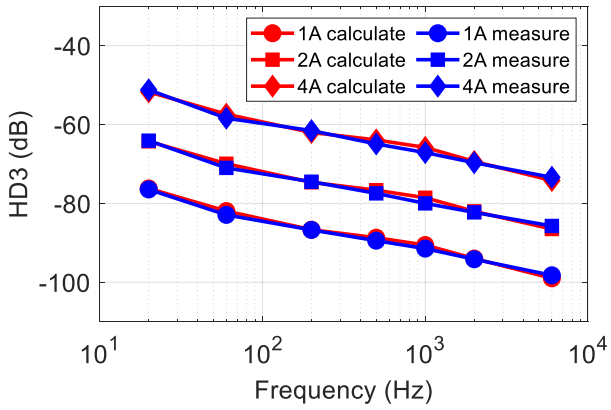

Fig. 13. Measured HD3 and calculated HD3 versus frequency in different current amplitudes.

V. Conclusion

This paper presents a test structure for a 27 mΩ diffusion current sensing resistor, designed to analyze distortion caused by self-heating. The parallel Kelvin connection minimizes parasitic effects from metals and vias, limiting resistance error to 0.4% and tc error to 0.7%. The diode array monitors and averages temperature variations across the resistor. According to those results, the HD3 from self-heating is characterized by an inaccuracy of 1.4 dB, and this distortion is compensated by at least 15dB through the sensed average temperature.

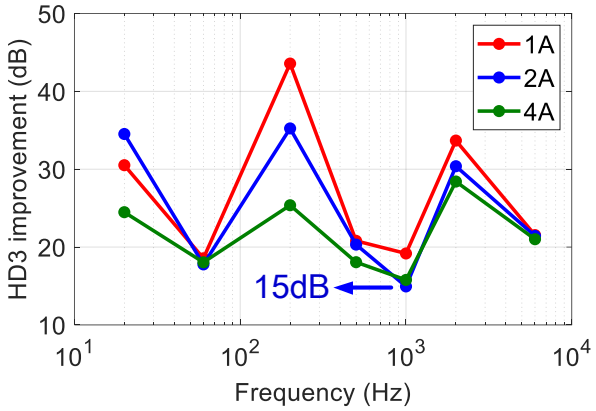

Fig. 14. HD3 compensation through the sensed average temperature of the diode array.

References

[1] Texas Instruments, "Current Sense Amplifiers in Class-D Audio Subsystems," Application Brief SLYA031A, July 2022. [Online]. Available: https://www.ti.com/lit/ab/slya031a/slya031a.pdf.

[2] V. Binet, F. Amiard, E. Allier, S. Valcin and A. Nagari, "A fully integrated Class-D amplifier in 40nm CMOS with dynamic cascode bias and load current sensing," *ESSCIRC 2014 - 40th European Solid State Circuits Conference (ESSCIRC)*, Venice Lido, Italy, 2014, pp. 319-322, doi: 10.1109/ESSCIRC.2014.6942086.

[3] A. Nagari, E. Allier, F. Amiard, V. Binet and C. Fraisse, "An 8 Ω 2.5 W 1%-THD 104 dB(A)-Dynamic-Range Class-D Audio Amplifier With Ultra-Low EMI System and Current Sensing for Speaker Protection," in *IEEE Journal of Solid-State Circuits*, vol. 47, no. 12, pp. 3068-3080, Dec. 2012, doi: 10.1109/JSSC.2012.2225762.

[4] M. Berkhout, L. Dooper and B. Krabbenborg, "A 4Ω 2.65W Class-D Audio Amplifier With Embedded DC-DC Boost Converter, Current Sensing ADC and DSP for Adaptive Speaker Protection," in *IEEE Journal of Solid-State Circuits*, vol. 48, no. 12, pp. 2952-2961, Dec. 2013, doi: 10.1109/JSSC.2013.2284692.

[5] Texas Instruments, TAS2764 Datasheet. [Online]. Available: https://www.ti.com/product/TAS2764.

[6] L. Xu, J. H. Huijsing and K. A. A. Makinwa, "A ±4A high-side current sensor with 25V input CM range and 0.9% gain error from −40°C to 85°C using an analog temperature compensation technique," *2018 IEEE International Solid-State Circuits Conference - (ISSCC)*, San Francisco, CA, USA, 2018, pp. 324-326, doi: 10.1109/ISSCC.2018.8310315.

[7] M. Mauerer, A. Tüysüz and J. W. Kolar, "Voltage/current measurement performance and power supply rejection in all-digital Class-D power amplifiers," *IECON 2016 - 42nd Annual Conference of the IEEE Industrial Electronics Society*, Florence, Italy, 2016, pp. 666-673, doi: 10.1109/IECON.2016.7793041.

[8] E. Simo, "Resistor non-linearity – there's more to Ω than meets the eye," Linear Audio, vol. 1, Apr. 2011, pp. 138-146. [Online]. Available: https://linearaudio.net/resistor-non-linearity-theres-more-ohm-meets-eye.

[9] Texas Instruments, "TAS2781 24-V Class-D Amplifier with Real Time Integrated Speaker Protection and Audio Processing datasheet (Rev. B)" Texas Instruments, 2013. [Online]. Available: https://www.ti.com/lit/ds/symlink/tas2781.pdf?ts=1732842782920.

[10] H. Zhang, S. Karmakar, L. J. Breems, M. Berkhout, K. A. A. Makinwa, and Q. Fan, "A High Linearity and Low-EMI Multilevel Class-D Amplifier," *IEEE Journal of Solid-State Circuits*, vol. 56, no. 4, Apr. 2021, pp. 1176-1185, doi: 10.1109/JSSC.2020.3043815.

[11] M. Chu, T. Harjono, K. Joardar, and V. Krishnamurthy, “Modeling and Test Structures for Accurate Current Sensing in Vertical Power FETs,” *2019 IEEE International Conference on Microelectronic Test Structures (ICMTS)*, Kita-Kyushu, Japan, 2019, pp. 102-106, doi: 10.1109/ICMTS.2019.8730949.

[12] Texas Instruments, “Low Temperature Drift Integrated Shunt vs Active Temperature Compensation of Shunt,” *TechNotes* SLYA032, Dec. 2017. [Online]. Available: https://www.ti.com/lit/ab/slya032/slya032.pdf.

[13] S. Pan, Y. Luo, S. H. Shalmany and K. A. A. Makinwa, “A Resistor-Based Temperature Sensor With a 0.13 pJ·K^2 Resolution FoM,” *IEEE Journal of Solid-State Circuits*, vol. 53, no. 1, Jan. 2018, pp. 164-173, doi: 10.1109/JSSC.2017.2746671.

[14] S. -H. Wen, C. -H. Hsiao, S. -H. Chien, Y. -C. Chen, K. -H. Chen and K. -D. Chen, "A −117dBc THD (−132dBc HD3) and 126dB DR Audio Decoder with Code-Change-Insensitive RT-DEM Algorithm and Circuit Technique for Relaxing Velocity Saturation Effect of Poly Resistors," *2022 IEEE International Solid-State Circuits Conference (ISSCC)*, San Francisco, CA, USA, 2022, pp. 482-484, doi: 10.1109/ISSCC42614.2022.9731634.

[15] A. Ito, “Modeling of voltage-dependent diffused resistors,” *IEEE Transactions on Electron Devices*, vol. 44, no. 12, Dec. 1997, pp. 2300-2302, doi: 10.1109/16.644657.

[16] Ken Kundert, “Modeling Diffusion Resistors,” [Online]. Available: https://designers-guide.org/modeling/diffusion-resistors.pdf.

[17] C. P. L. van Vroonhoven and K. A. A. Makinwa, "Thermal diffusivity sensing: A new temperature sensing paradigm," *2011 IEEE Custom Integrated Circuits Conference (CICC)*, San Jose, CA, USA, 2011, pp. 1-6, doi: 10.1109/CICC.2011.6055368.